Biosensors and Bioelectronics 270 (2025) 116977

Contents lists available at ScienceDirect

Biosensors and Bioelectronics

journal homepage: www.elsevier.com/locate/bios

Small-scale magnetic soft robotic catheter for *in-situ* biomechanical force sensing

Ruirui Li [a], Jun Wang [a], Xuhui Zhao [b], Zonglian Liu [c], Pinggang Jia [a], Yuan Liu [b,**], Gungun Lin [d,*], Haifeng Xu [b,***], Jijun Xiong [a]

[a] State Key Laboratory of Dynamic Measurement Technology, North University of China, Taiyuan, 030051, China
[b] Shenzhen Institute of Advanced Technology, Chinese Academy of Sciences, Shenzhen, Guangdong Province, 1068 Xueyuan Avenue, 518055, China
[c] Department of Cardiology, Zizhong People's Hospital, Neijiang, 641200, China
[d] Institute for Biomedical Materials and Devices, School of Mathematical and Physical Sciences, Faculty of Science, University of Technology Sydney, Sydney, 2007, New South Wales, Australia

A B S T R A C T

Miniaturized magnetic soft robotic catheters offer significant potential in minimally invasive surgery by enabling remote active steering and reduced radiation exposure. However, existing magnetic catheters are limited by the absence of *in-situ* biomechanical force sensing, which is crucial for controlling the contact force exerted on surrounding tissues during surgical procedures. Here, we report an *in-situ* force sensing strategy for small-scale magnetic robotic catheters. A coaxial integration of ring-shaped permanent and fibre-based force sensors at the catheter's distal end enables both active steering and precise force measurement. The force sensor is designed to be sensitive exclusively to contact forces perpendicular to its plane, achieving a sensitivity of 0.69 nm/kPa (or 0.38 nm/mN). By manipulating magnetic field patterns, the catheter can actively generate and control contact forces to tissues, using real-time feedback from the force sensor. We demonstrate the system's force-sensing and force-control capability in isolated organs and tissue phantom during passage, verifying the catheter's high force sensitivity and high steerability. The feedback-loop force control enhances procedural safety and efficacy for minimally invasive surgery, making it especially suitable for procedures such as transbronchial microwave ablation of lung nodules and cardiac ablation for atrial fibrillation.

1. Introduction

Minimally invasive surgery is increasingly favored for its ability to minimize trauma and shorten recovery times for patients (Yang et al., 2023). Miniaturized catheters and guidewires offer significant potential for therapeutic and diagnostic interventions within small lumens (Zhou et al., 2021). To optimize steerability and improve procedural outcomes in these confined spaces, multi-functional capabilities – such as active steering (Yang et al., 2022; Zhang et al., 2021), variable stiffness (Piskarev et al., 2024; Agno et al., 2023), and unclogging motion (Lee et al., 2021; Li et al., 2024) - are necessary for soft catheters and guidewires. Magnetic soft catheters and guidewires, which are driven by external magnetic field are known for their high penetrability and biosafety, offer effective active steering within small lumens (Yang et al., 2020, 2022; Kim et al., 2022; Azizi et al., 2019; Hong et al., 2021; Kuntz et al., 2022).

A notable example of this is Zhao et al.'s development of magnetic soft catheters, created by incorporating magnetic microparticles into a soft matrix (e.g., TPU and PDMS) (Kim et al., 2019). These catheters are capable of aligning their distal ends with the orientation of the magnetic field, facilitating precise navigation. By integrating the optical fibre into the catheterter as a functional core, these catheters provide an additional capability for steerable laser delivery. Moreover, small integrable permanent magnets (ranging from micrometer to millimeter scale) have been widely utilized in magnetic soft catheters due to their high magnetization (Tiryaki et al., 2023). For instance, Tiryaki et al. integrated neodymium magnets at the distal end of an optical fiber rod, allowing magnetic steering within a 7-T MRI scanner (Tiryaki et al., 2023). During magnetic steering and navigation, the interaction between the catheter's distal end and the surrounding generates a contact force. Excessive contact force, however, can cause significant mechanical damage to the lumen channel. Currently, the passage of catheters primarily relies on the surgeon's tactile feedback, making it challenging to quantify the forces at the distal end (Lou et al., 2010). This is problematic for ablation procedures (e.g., transbronchial microwave ablation of lung nodules (Hu et al., 2024) and cardiac ablation for atrial

* Corresponding author.
** Corresponding author.
*** Corresponding author.
E-mail addresses: y.liu1@siat.ac.cn (Y. Liu), gungun.lin@uts.edu.au (G. Lin), hf.xu@siat.ac.cn (H. Xu).

https://doi.org/10.1016/j.bios.2024.116977
Received 28 September 2024; Received in revised form 10 November 2024; Accepted 19 November 2024
Available online 20 November 2024

fibrillation (Natale et al., 2014; Wang et al., 2022), where precise force control based on real-time feedback is essential to improving procedural outcome.

Force sensing enables feedback on the contact force between the catheter's distal end and surrounding tissue, making force control feasible. Existing force-sensing strategies can be classified into two major categories: theoretical modelling (Wang et al., 2022) and physical force sensors (Lou et al., 2010). The former strategy typically relies on simplifying assumptions. For instance, Wang et al. used a programmed magnetic field to steer the distal end of a magnetic guidewire, estimating the force level using the finite difference method (Wang et al., 2022). However, this model assumes that the influence of friction and sliding between the distal end and tissue are negligible, which may limit its accuracy. In contrast, miniaturized force sensors provide direct detection of contact forces, offering more reliable and precise feedback. These sensors such as piezoresistive, capacitive, and piezoelectric sensors, convert the applied force into electrical signals for real-time monitoring (Lou et al., 2010). Notably, Lou et al. utilized a cantilever-based piezoresistive sensor to measure contact forces (Lou et al., 2010). However, to ensure functionality within small lumens, including blood vessels, an encapsulation layer is required to isolate the sensor's electrical components from the surrounding fluid.

Here, we introduce a contact force-sensing mechanism for magnetic soft catheters. The catheter integrates an optical fibre force sensor and a permanent magnet, enabling active steering under low magnetic field conditions. The *in-situ* force sensing capability provides real-time feedback during the passage of the magnetic cathether (Fig. 1). Upon reaching the lesion site, the distal end of the catheter facilitates precise control of contact force generation. The microfabricated force sensor exhibits high sensitivity (0.69 nm/kPa = 0.38 nm/mN) and maintains

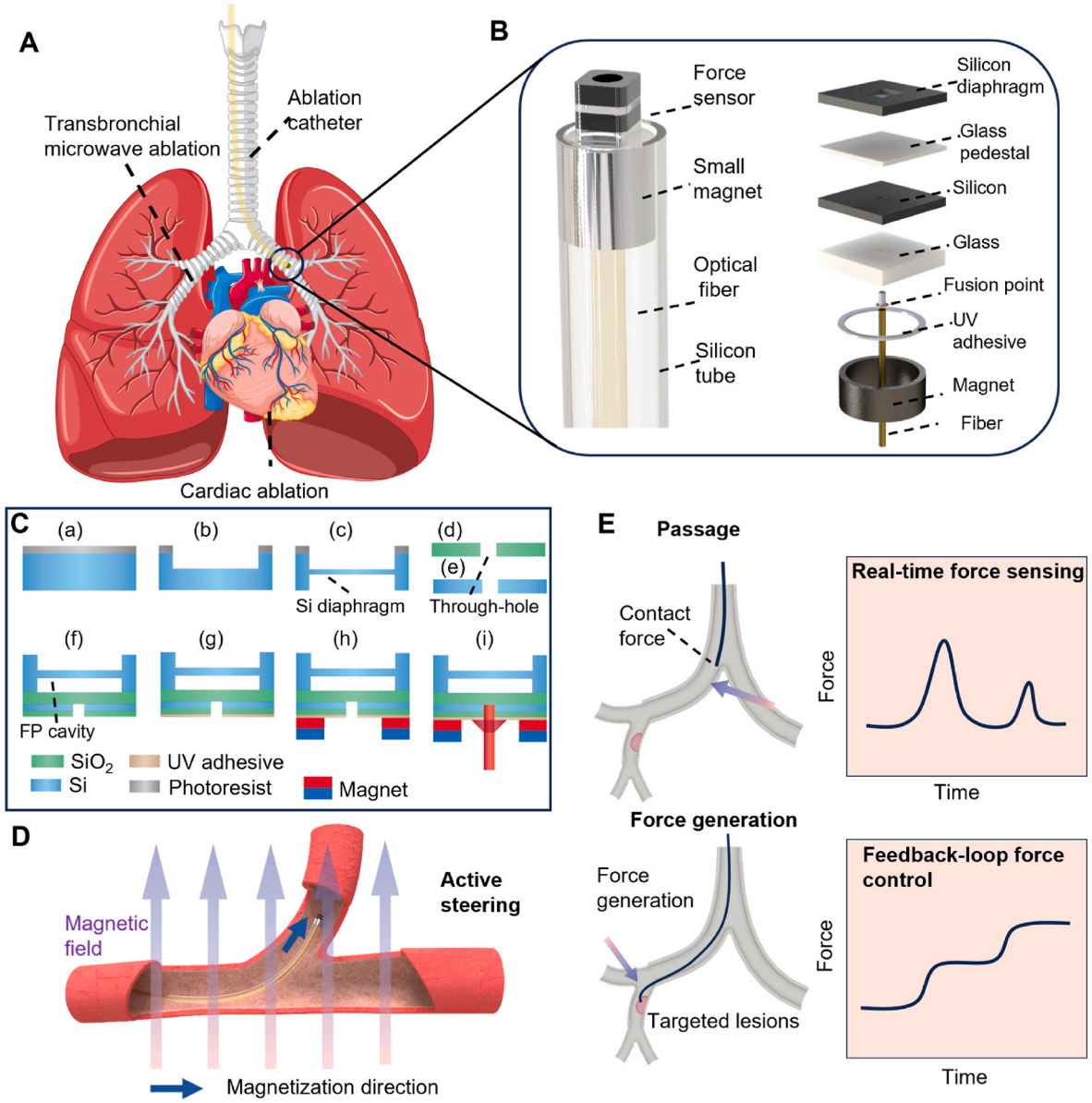

Fig. 1. Schematic representation of ablation using magnetic robotic catheters. (A) Surgical application scenarios of the magnetic catheter, including transbronchial microwave ablation of lung nodules and cardiac ablation for atrial fibrillation. (B) Diagram of the soft catheter, highlighting the integration of a force sensor and a ring-shaped magnet. (C) The manufacturing process of the magnetic catheter includes the following steps: a. Spin-coating photoresist onto the silicon wafer. b-c. Deep etching on both sides of the silicon wafer. d-e. Fabrication of through-holes on the silicon wafer and glass wafer. f. Anodic bonding of the force sensor. g-h. Adhesive bonding between the force sensor and the magnet. i. Securing the optical fiber using fusion points. The catheter provides multiple functionalities, including magnetic steering (D) force sensing during navigation, and feedback control of contact force generation (E).

high stability when in contact with surrounding fluid and tissue. We demonstrate the catheter's primary capability, including active steering and force feedback, in both a bronchial phantom and an isolated organ model. Additionally, controlled force generation is validated in an isolated pig's heart. This high-sensitive and stable force sensing approach holds significant potential for minimizing mechanical damage and enabling precise contact force control during surgical procedures, such as ablations for atrial fibrillation (Wang et al., 2022) and lung cancer treatments (Rose et al., 2006), within small lumens.

2. Results and discussions

2.1. Fabrication of magnetic soft catheters

The magnetic soft catheter comprises two important components: the force sensor and the ring-shaped magnet (Fig. 1B and C). The force sensor was fabricated using microfabrication and a glass-silicon bonding process. The optical fiber sensor comprises a silicon diaphragm, a glass pedestal, and a flexible optical fiber. The silicon diaphragm was created

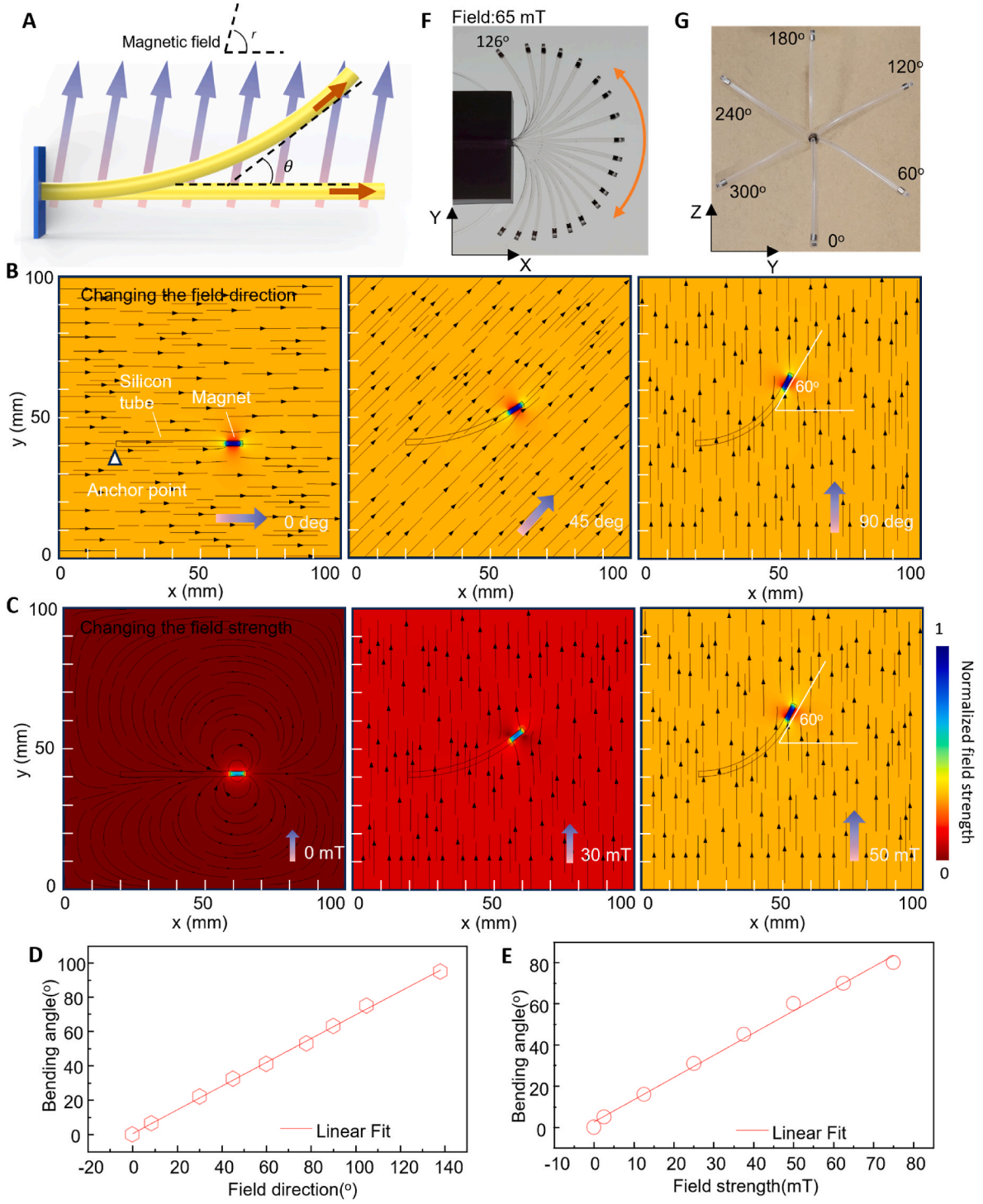

Fig. 2. Characterization of magnetic steering. (A) Schematic of the magnetic bending under an external magnetic field. The red arrow is the magnetization direction of the ring-shaped magnet. The red-to-blue arrows represent the external magnetic field. (B–D) Simulation of bending actuation under various field directions and field intensities. Bending actuation with various curvatures (F) and directions (G).

by deep silicon etching on both sides of the silicon film. A metal film coated on the back side of the silicon diaphragm enhanced the light reflectivity. A Fabry-Perot (FP) cavity was created by bonding the silicon film with the glass pedestal. The optical fibre was directly integrated into the force-sensing structure to transmit force signals, with the flexible fibre fixed at the fusion point via a CO_2 laser. The width of the force sensor is scalable due to the high-resolution microfabrication technology. For this study, the sensor was designed with a width of 2 mm to accommodate the dimension of small lumens (e.g., the sixth bronchi with diameter <3 mm) (Makevnina, 2018).

A ring-shaped permanent magnet, approximately 2.3 mm in diameter, serves as the magnetic component for steering the catheter's distal end. The force sensor and magnet were coaxially integrated within a silicone tube, with the magnet fixed at the base of the sensor using the UV adhesive. This configuration ensures that the force sensor maintains direct contact with the tissue, thereby minimizing the impact of the distal end bending on the force sensing. Otherwise, the magnet is positioned at the front side of the force sensor, preventing direct detection of contact forces by the silicon diaphragm. Additionally, the presence of the magnet increases the diaphragm's thickness, resulting in reduced sensitivity.

2.2. Characterization of magnetic steering capability of soft catheter

Remote magnetic steering is achieved by aligning the distal end of the magnetic soft catheter with the direction of the external field (Fig. 2A). The field is generated by a moving magnet, measuring 15 mm in diameter and 20 mm in height. The ring-shaped magnet embedded at the distal end of the magnetic soft catheter is axially magnetized. When exposed to the external magnetic field, the distal end experiences a magnetic torque, allowing precise steering:

$$T = M \times B = MBsin(r - \theta) \tag{1}$$

where M is the dipole moment, B is the field strength of the magnetic field, r is the field direction of the magnetic field, and θ is the orientation of the distal end. The distal end bends to a specific angle until the magnetic dipole moment is aligned with the magnetic field.

We employed a finite element analysis (FEA) to optimize and guide the magnetic steering of the catheter (Fig. 2B–**2E**). In the COMSOL simulation, the magnetic catheter consists of a silicon beam and a permanent magnet. The diameter of the silicon tube is 2.5 mm, and the elastic modulus is 50 MPa. The magnet fixed at the distal end possesses a residual magnetization of 100 mT. For the magnetic field, we use an external field (0∼100 mT) to generate the magnetic torque and bend the distal end. By adjusting the field direction and strength, we observed the catheter's bending behaviour. The distal end experiences a magnetic torque under the external magnetic field, with the bending angle increasing to 60° as the field strength is increased from 0 to 50 mT. The bending of the magnetic soft guidewire can be controlled by changing the field direction. Simulation results confirm the feasibility of active steering through the integration of a ring-shaped permanent magnet at the distal end.

Fig. 2F shows the various curvatures of the catheter tip, with the bending angle increasing linearly as the field direction changes from −150° to 150°. The bending angle reaches 126° under a field strength of 65 mT. Fig. 2G demonstrates bending in different directions at a fixed curvature. The active bending capability with diverse curvatures and directions underscores the catheter's potential for steering its distal end in arbitrary directions under a magnetic field. These results confirm the high steerability of the magnetic soft catheter.

2.3. Force response characterization

The force sensor was characterized within a pressure tank, where the pressure applied to the sensor surface could be precisely modulated (range: 0∼10 MPa, pressure control accuracy: 0.5% of full scale (FS)) by adjusting the nitrogen (N_2) pressure in the tank (Fig. 3A and B). The N_2 pressure simulates the tactile pressure exerted on the tissue.

The Febry-Perot cavity was constructed between the fibre end and the inner surface of the silica diaphragm, where multi-beam interference occurs. When pressure is applied, the sensitive silicon diaphragm deforms, resulting in a change in the cavity length L. This deformation causes a noticeable shift in the interference peaks, which can be measured using a spectrometer (Fig. 3D). The change in cavity length can be calculated through the spectra:

$$\nabla L = \frac{\lambda_{1o}\lambda_{2o}}{2(\lambda_{1o} - \lambda_{2o})} - \frac{\lambda_1\lambda_2}{2(\lambda_1 - \lambda_2)} \tag{2}$$

Where λ_{1o} and λ_{2o} are wavelength values corresponding to adjacent peaks or troughs with zero pressure, and λ_1 and λ_2 are wavelength values corresponding to adjacent peaks or troughs under a specific pressure.

The change in cavity length under a specific pressure P or force F can be calculated and expressed as follows:

$$\nabla L = \frac{3(1-\mu^2)R^4}{16Eh^3}P = \frac{3(1-\mu^2)R^2}{16\pi Eh^3}F \tag{3}$$

where P and F are the pressure on the surface of the sensitive silicon diaphragm, E and μ are Young's modulus and Poisson's ratio, h is the thickness of the silicon diaphragm, and R is the radius of the silicon diaphragm.

Previous studies suggest that a contact force range of 0.1∼0.4 N is necessary to optimize the outcome of cardiac ablation. To meet this requirement, we designed the force sensor with a linear response range of 0∼1 N. The thickness and radius of the sensitive silicon diaphragm are key factors in determining the upper limit of its linear deformation ($\nabla L_{max} \leq 0.3h$). Consequently, the force response range can be expressed as:

$$F_{max} \leq \frac{1.6\pi Eh^4}{(1-\mu^2)R^2} \tag{4}$$

Based on the above relationship, the thickness of the silicon diaphragm can be calculated as follows:

$$h \geq \frac{(1-\mu^2)R^2}{1.6\pi E}F_{max} \tag{5}$$

For a silicon diaphragm with a radius of 1.2 mm, the corresponding diaphragm thickness of 63 μm yields a contact force sensing range of 0∼1 N (0∼884 kPa). This design allows for adjusting sensor parameters to accommodate various force response requirements, depending on specific surgical scenarios.

We defined the sensitivity as the ratio of the length change in the cavity to the pressure (or the force)

$$S = \frac{\nabla L}{P} = \frac{3(1-\mu^2)R^4}{16Eh^3} \text{ or } S = \frac{\nabla L}{F} = \frac{3(1-\mu^2)R^2}{16\pi Eh^3} \tag{6}$$

The theoretical sensitivity is 0.692 nm/kPa through equation (6) (E = 129.5 GPa, μ = 0.278). We also use the FEA method to simulate the deflection of the silicon diaphragm under constant pressure. The deflection is 0.697 nm under the pressure of 1 kPa, resulting in a sensitivity of 0.697 nm/kPa in the simulation (Fig. 3C).

In the experiments, we recorded the cavity length under different pressures. The cavity length exhibited a linear decrease with increasing applied pressure, as depicted in Fig. 3E. This sensor demonstrates high-force sensitivity (0.69 nm/kPa) and a low non-linearity error (0.17 % FS), with the actual sensitivity closely matching the theoretical value. To assess repeatability, pressures ranging from 0 to 900 kPa were applied in 100 kPa intervals, with each measurement repeated three times (Fig. 3F). A small difference in sensitivity was observed among the three tests. The regression coefficient (R^2) between the cavity length and applied pressure exceeded 0.999, indicating that the force sensor

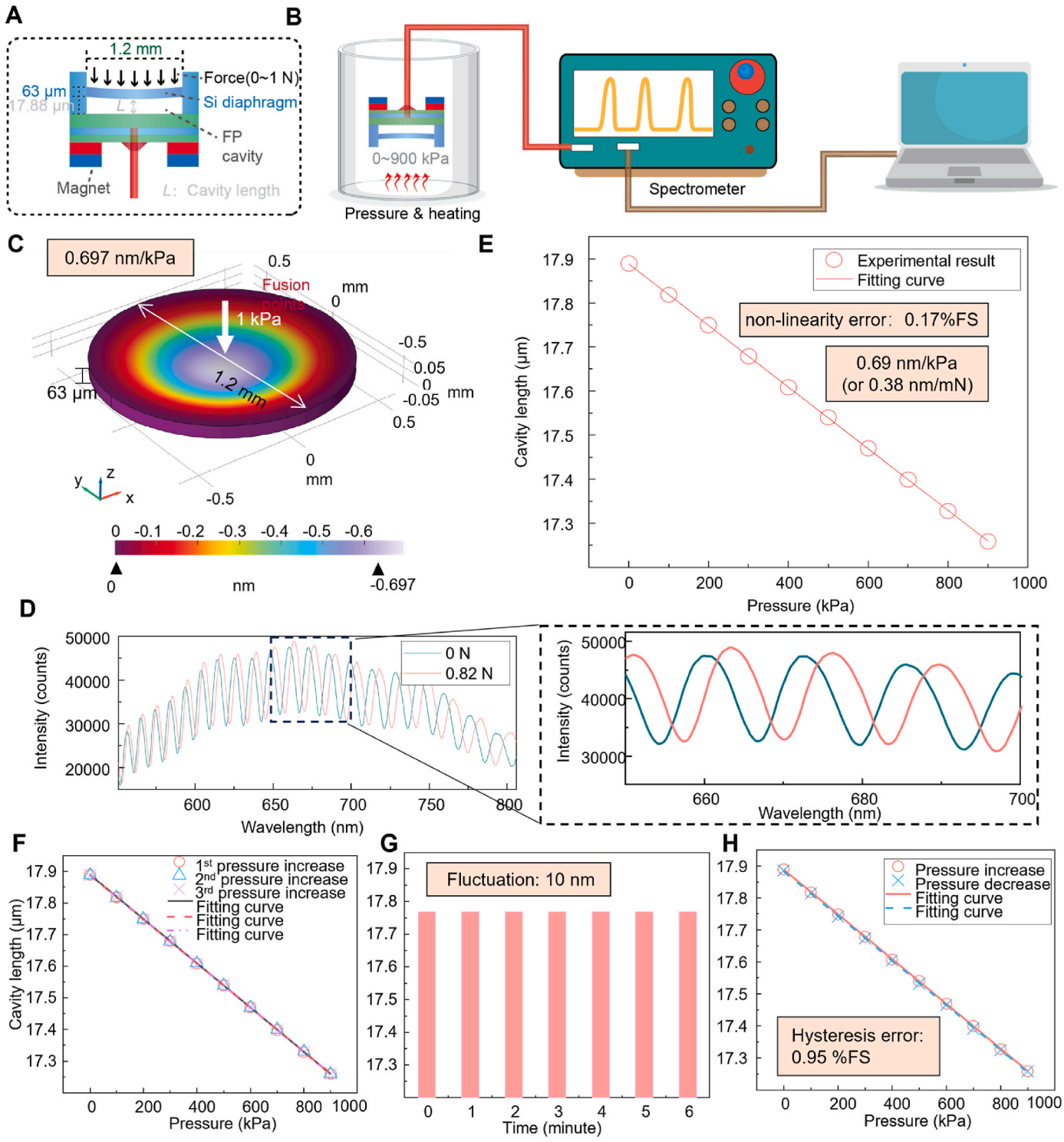

Fig. 3. Force response characterization. (A) Schematic illustration of force sensor. (B) Schematic illustration of force sensor of force response test system. (C) Simulation of deflection of the silicon diaphragm under pressure. (D) Sensor spectra. The right panel is the shift of the spectra under 0.82 N force. (E) Force sensing range. (F–G) The repeatability, stability, and hysteresis of the force sensor under pressure.

exhibited excellent repeatability. In addition, the sensor has a stable output of 17.76 μm in cavity length at a constant pressure of 200 kPa. The fluctuation of the cavity length (the difference between the maximum length and minimum length) is ~10 nm within 6 min (Fig. 3G). Moreover, the sensor showed a low hysteresis error of 0.95 % FS when the load was increased and decreased, indicating rapid response to external forces (Fig. 3H). The sensor's outstanding performance in terms of sensitivity, stability, repeatability, and hysteresis, highlights its potential for accurate contact force sensing during surgical procedures.

2.4. *In-situ force sensing in a bronchus phantom*

We first demonstrate the fundamental force-sensing capability using an isolated lung organ to map the contact force. The magnetic catheter was fixed in a linear stepping motor, which allows movement along the

Z-axis (2 mm displacement) to contact the tissue. The catheter was then repositioned to different points to test contact force. Fig. 4A illustrates the force mapping of multiple points on the lung surface, confirming the feasibility of the contact force sensing. The contact force is 57.4∼73.7 mN. We further used the catheter to locate the tumour phantoms (Fig. 4B). We used hydrogel to mimic tissue, embedding high-stiffness objects within it to simulate tumors. The catheter moved horizontally in 5-mm intervals, pressing the phantoms to a depth of 2 mm. The contact force values on the hydrogel were measured to be less than 39.1 mN, while the force values on the high-stiffness objects exceeded 290.0 mN. This difference in force can be used to outline the lump phantoms, which include both ring-shaped and disk-shaped structures. The catheter successfully identified the 5-mm diameter hole in the ring-shaped lump. The mechanical feedback capability of the catheter shows great potential in assessing the mechanical properties of different tissue regions and determining health status.

The *in-situ* force sensing capability was further demonstrated using a bronchus phantom. During the catheter's passage, the silicon diaphragm is sensitive only to the normal force. To prevent magnetic steering from affecting force sensing, the magnet is securely fixed at the base of the force sensor. When the distal end interacts with tissue, it experiences two types of forces: contact force and frictional force. To enhance the catheter's lubricity and reduce the impact of surface friction on force sensing, a hydrophilic coating is applied to its surface. This coating ensures smoother navigation and more accurate force measurements by minimizing friction-related interference. The contact force at the interface between the distal end of the magnetic catheter and the tissue can be divided into normal and tangential components. The normal component of the contact force is particularly important, as it plays a critical role in determining the extent of mechanical damage at the contact point. In the experiment, the catheter initially approaches the bifurcation without applying an external magnetic field (Fig. 4C). Upon reaching the bifurcation, the distal end contacts the channel wall. and the force value was recorded (260 mN) from the force response curve. A magnetic field was then applied to bend to the distal to the right channel. A 30 mT magnetic field induces a 30-degree deflection angle, facilitating the catheter's passage. As the field strength gradually increased, the distal end bent slowly, with minimal contact force during bending, indicating that the effect of bending on force sensing was negligible. The catheter continued to advance until it contacted the channel wall at a second bifurcation, where a force value of 165 mN was recorded. The *in-situ* force-sensing capability ensures that the applied force remains within a safe range when contacting the lumen wall.

We recorded force values as the catheter navigated through an isolated pig's bronchus (Fig. 4D). Initially, as the catheter is inserted, the force remains close to zero. Upon reaching a bifurcation and contacting the lumen wall, however, the force rises sharply to approximately 0.2 N. To traverse the bifurcation, we adjusted the magnetic field direction (30 mT), enabling the magnetic catheter to avoid obstacles. Once the distal end circumvents the obstruction and enters the branch through magnetic steering, the force value returns to zero. These results demonstrate the magnetic catheter's capability to navigate bifurcations effectively using magnetic steering and real-time force feedback.

2.5. Feedback-loop force control in ex-vivo organ

We further demonstrated the precise control of contact force using the isolated pig's heart model. Previous reports indicate that a contact force in the range of 0.1∼0.4 N improves ablation outcomes (e.g., cardiac ablation). When the distal end comes into contact with the tissue, the applied force in the normal direction is crucial for performing the ablation effectively. Magnetic steering ensures the distal end can reach the targeted area. The force feedback allows us to control the force applied to the tissue based on localized force sensing. The contact force is regulated by adjusting the load by increasing the strength of the external magnetic field (Fig. 5A). For example, with the distal end in contact with the target lesion under the influence of a magnetic field, a contact point was established between the distal end and the targeted lesion. By decreasing the distance between the moving magnet and the ring-shaped magnet at the distal end, the field strength was increased (∇B), resulting in a higher contact load ($F\sim \nabla B$). The field direction stays the same to keep the location of the contact point.

The feedback-loop control algorithm modulates the load based on real-time force feedback. In the experiment, we guided the catheter to the atrium using magnetic steering. Initially, at the point of contact, no measurable contact force was present. The external magnet, mounted on a mechanical slide table, acted as the field generator, allowing precise control over both the field direction and strength. The system is capable of generating a magnetic field of up to 600 mT. By increasing the magnetic field strength, the contact force quickly rose to 0.2 N. Once the load reached the desired value (e.g., 0.2 N), the external magnet was held in place, and the distance between the external and ring-shaped magnets was maintained, ensuring the contact force remained stable for 10 s (Fig. 5B and C). If the force deviates from the target value, the load is dynamically adjusted to restore and maintain the desired force level. Then we further increased the field strength, and the contact force was switched to 0.35 N. As shown in Fig. 5C, the contact force can be adjusted from 0 to 1 N to achieve specific values, such as 0.2 N, 0.35 N, 0.6 N, and 1 N. For instance, when targeting a force of 0.6 N, the actual force was maintained at 0.586 ± 0.03 N. The minimal fluctuation in contact force demonstrates the stability of the applied force. This precise force control highlights the effectiveness of the force-sensing mechanism in enabling feedback-loop control during surgical procedures.

3. Conclusion

We have developed a small-scall magnetic soft catheter and a method of sensing and feedback-loop control of contact force generated by the catheter. This innovative catheter integrates multiple functions, including magnetic active steering, *in-situ* force sensing, and feedback-loop force control. The ring-shaped magnet used in the magnetic soft catheter provides active steering during surgical procedures. The catheter can achieve a bending range of up to 126°, facilitating rapid navigation of the distal end.

The optical-fiber-based force sensing capability demonstrates high sensitivity (0.69 nm/kPa), accurately measuring contact force. The integrated force sensor at the distal end offers a broad force response range (0∼1 N) and maintains robustness even under substantial forces. The advancement of the magnetic soft catheter is facilitated by a linear motor, which dynamically adjusts the applied force through variations in magnetic field patterns. This integration of force sensing and active steering enables the distal end to generate a controlled contact force at any position. Such feedback-loop control of contact force is essential for enhancing safety and efficacy in ablation procedures.

The magnetic catheter demonstrates significant potential for tissue palpation, obstacle identification, and navigation. It performs tissue palpation by interacting with the tissue through its distal end, identifying stiffness variations via force mapping. When the catheter encounters a high-stiffness area, the force sensor provides feedback with elevated force values. The magnetic catheter is particularly sensitive to normal forces during its passage, allowing the distal end to detect obstacles through increased force readings. Active steering enables the catheter to avoid obstacles and continue navigating through lumens. Furthermore, automatic navigation of the magnetic catheter can enhance the efficiency of minimally invasive surgery. Force values serve as a critical index for this automated navigation. When the force value rises significantly, the catheter automatically responds by adjusting the magnetic field to circumvent the obstacle. Once the force value returns to near zero, the linear motor advances the catheter, facilitating continuous navigation.

The force sensor, fabricated using microfabrication technology, is millimeter-scale in size, making it ideal for applications in the bronchus

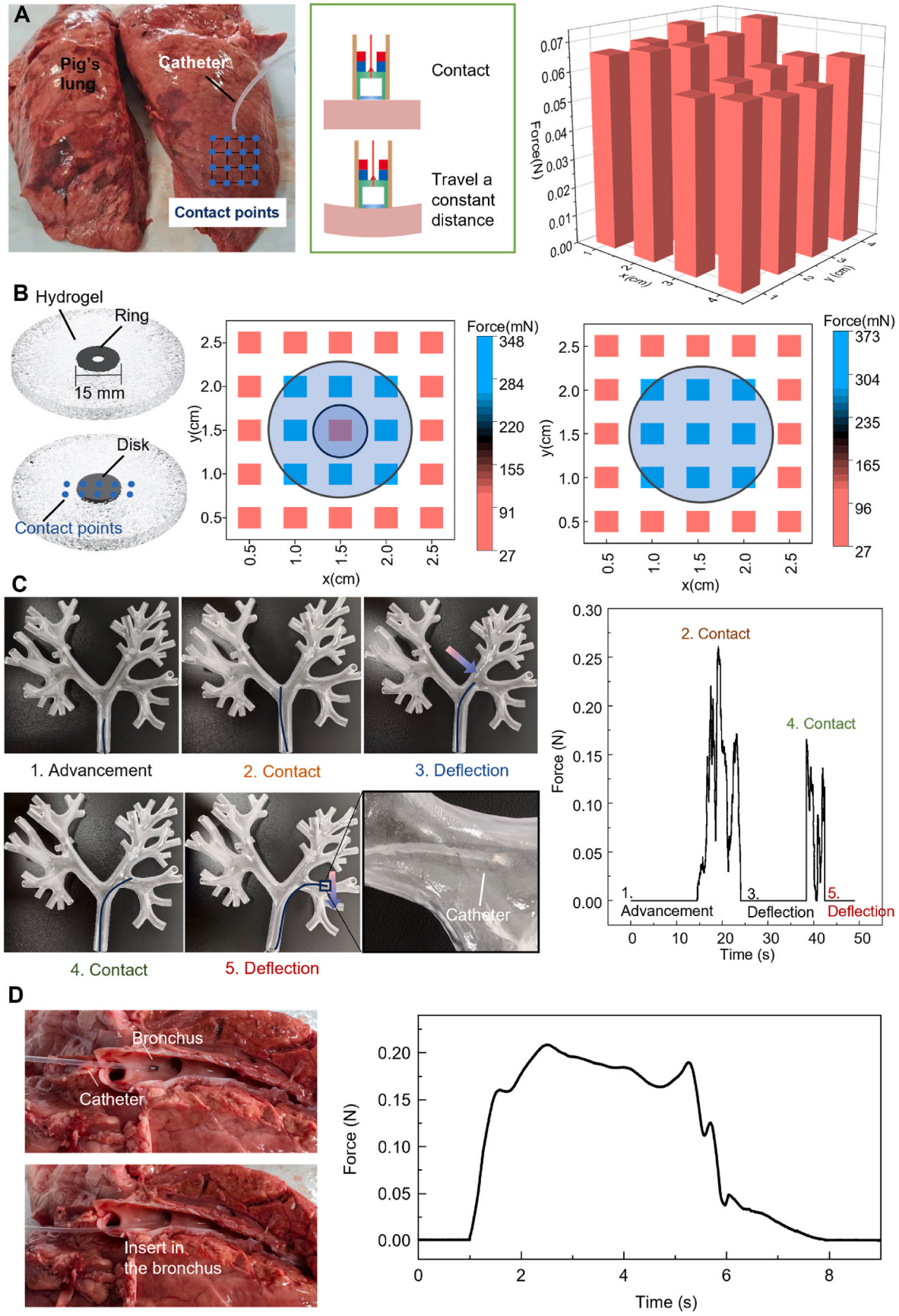

Fig. 4. *In-situ* force sensing. (A) Contact force mapping on the surface of the isolated lung organ. (B) Palpation on tumour phantoms. The hydrogel and high-stiffness objects (ring and disk shapes) were used to mimic the normal tissue and tumour. *In-situ* force sensing during the catheter passage in the bronchus phantom (C) and in the isolated bronchus model (D).

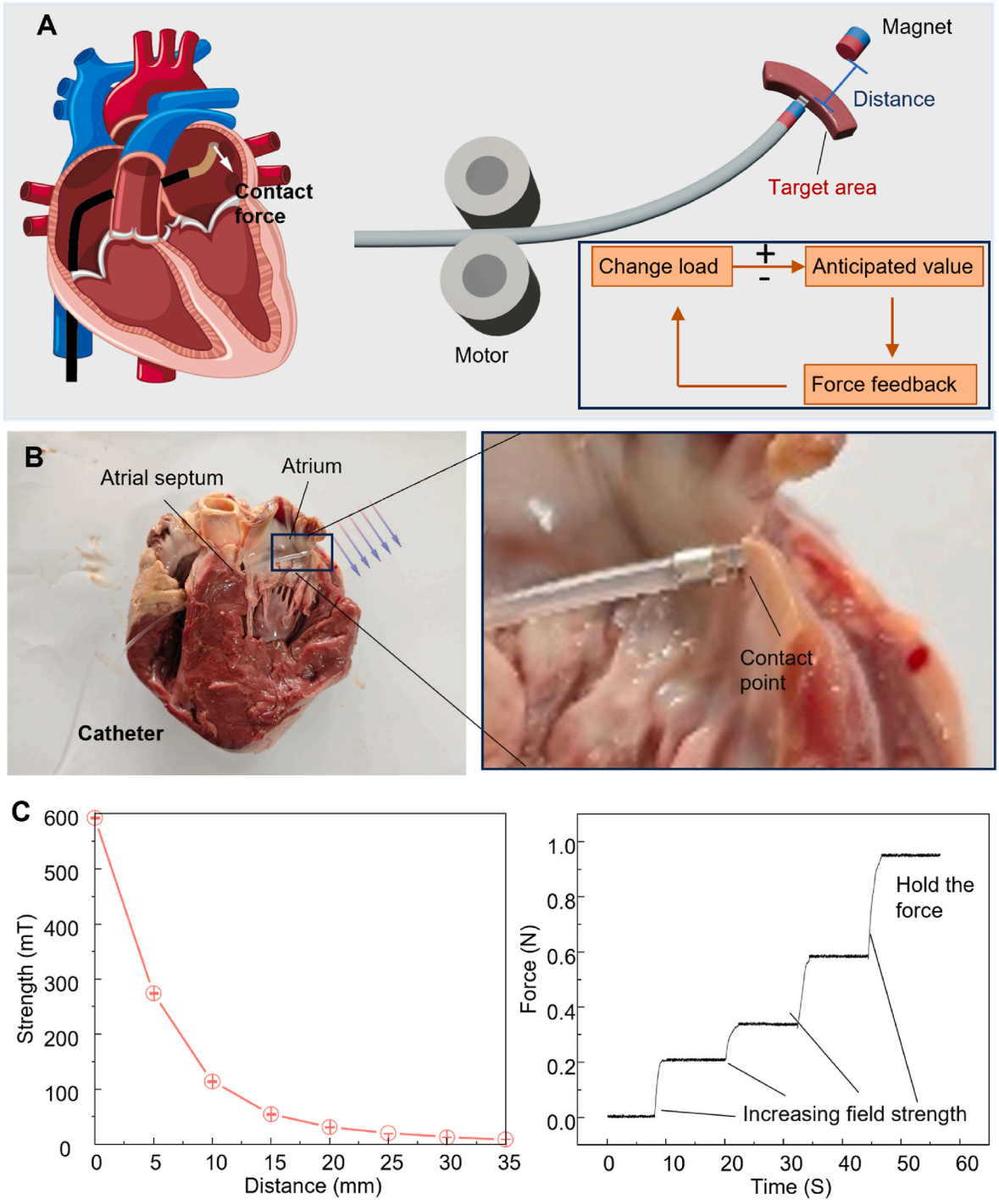

Fig. 5. Feedback-loop force control in the isolated pig's heart. (A) Schematic illustration of force generation for cardiac ablation. The inserted picture in the right panel is the feedback-loop control algorithm. (B) The magnetic catheter applies contact force to the left atrium. (C) Control force generation on the isolated heart. The left panel is the magnetic strength with the distance between the fibre's distal end and the external magnet. The right panel is the controlled force generation.

and cardiovascular systems. This fabrication approach offers scalability from micrometer to millimeter dimensions, enabling customization to meet specific application requirements. Additionally, microfabrication allows the force sensor to be produced in octagonal shapes, minimizing potential damage. Moreover, 3D photolithography with nano-scale fabrication resolution presents a promising method for creating round-shaped force sensors. This technique can directly integrate magnetic components by printing multiple materials. High-resolution fabrication methods have significant potential for developing magnetic catheters equipped with microscale force sensors and magnetic components. The diameter of the force sensor is crucial in determining its resolution. To achieve more precise tissue palpation, reducing the sensor's diameter can enhance the spatial resolution of force detection and improve overall performance.

4. Methods

Fabrication of force sensor: The optic fiber-based force sensor was fabricated by assembling a sensing structure and an optic fiber. Firstly, a circular silicon diaphragm with a diameter of 1.2 mm and thickness of

63 μm was prepared using photolithography and etching processes. After the anodic bonding of a 300 μm-thick quartz, the Fabry-Perot cavity for force sensing was achieved. A 500 μm-thick silicon with a through hole of 0.9 mm diameter was fabricated to align the silicon diaphragm. A 1 mm-thick quartz with a through hole of 130 μm diameter was prepared to fix the external optic fiber. Then the silicon and quartz with a through hole were bonded with the Fabry-Perot cavity structure. The bonded four-layer wafer was cut into a single unit with a width of 2 mm and a thickness of 2.1 mm. Subsequently, the optic fiber was inserted the through hole and fixed, and the optic fiber-based force sensor was achieved.

Fabrication of magnetic soft catheter: Based on the force sensor design, we employed a ring-shaped magnet as the magnetic component, which exhibits a residual magnetization of 100 mT. A hole was incorporated to allow the fiber to pass through. The ring-shaped magnet features an outer diameter of 2.3 mm, an inner diameter of 1 mm, and a length of 2.5 mm. A silicon tube was used for the coaxial assembly of the force sensor with the magnet. Additionally, UV adhesive was applied to bond the magnet at the base of the force sensor.

Magnetic steering: A magnetic field generator was developed using a cylindrical magnet (15 mm in diameter, 20 mm in height) fixed to a robotic arm. The direction of the magnetic field was controlled by adjusting the orientation of the cylindrical magnet, while the field strength was modulated by varying the distance between the cylindrical magnet and the ring-shaped magnet (0–100 mT). The catheter's advancement was driven by a linear motor, with speeds adjustable from 0 to 50 mm/s.

Force sensing characterization: The force sensors were characterized in a controlled pressure tank, where the surface pressure was regulated using nitrogen (N_2). A fiber-optic connector linked the flexible fiber to a spectrometer, which monitored the position of the interference peak. Changes in the cavity length, induced by external forces, caused shifts in the interference peak, allowing the cavity length to be calculated based on the peak shift.

Fabrication of hydrogel tumour model: Firstly, Acrylamide (AAM), 200 μL of N, N′-Methylenebisacrylamide (MBAA) aqueous solution (0.01 g/mL), 5 mL of potassium persulfate (KPS) aqueous solution (0.01 g/mL) were added to DI water and stirred under an ice bath for 20 min. After that, 100 μL of crosslinker N,N,N′,N′-Tetramethylethylenediamine (TEMED) was added to the aforementioned mixture and stirred under an ice bath for 1 min. Then, the prepared solution was poured into a culture dish and naturally polymerised for 2 h at room temperature to obtain the PAM hydrogel.

CRediT authorship contribution statement

Ruirui Li: Writing – original draft, Validation, Methodology, Investigation, Data curation. **Jun Wang:** Writing – review & editing, Writing – original draft, Visualization, Validation, Methodology, Investigation, Formal analysis, Data curation. **Xuhui Zhao:** Writing – original draft, Visualization, Methodology, Investigation, Formal analysis, Data curation. **Zonglian Liu:** Validation, Methodology. **Pinggang Jia:** Validation, Methodology. **Yuan Liu:** Writing – review & editing, Writing – original draft, Visualization, Supervision, Project administration, Funding acquisition, Formal analysis, Conceptualization. **Gungun Lin:** Writing – review & editing, Visualization, Methodology, Conceptualization. **Haifeng Xu:** Writing – review & editing, Visualization, Supervision, Methodology, Funding acquisition, Conceptualization. **Jijun Xiong:** Writing – review & editing, Supervision, Resources, Methodology, Funding acquisition.

Declaration of competing interest

The authors declare that they have no known competing financial interests or personal relationships that could have appeared to influence the work reported in this article.

Acknowledgment

National Natural Science Foundation of China 52203152, National Natural Science Foundation of China 52205610, National Natural Science Foundation of China 52303167, Australian Research Council DECRA Fellowship DE230100079, Opening Foundation of State Key Laboratory of Dynamic Measurement Technology 2022-SYSJJ-04, Shenzhen Outstanding Talents Training Fund RCBS20210706092255078, Shenzhen Outstanding Talents Training Fund RCBS20221008093222008, Shenzhen Science and Technology Program JCYJ20220818101409021, Shenzhen Science and Technology Program JSGGKQTD20221101115654021

Data availability

Data will be made available on request.

References

Agno, K.C., Yang, K., Byun, S.H., Oh, S., Lee, S., Kim, H., Kim, K., Cho, S., Jeong, W. Il, Jeong, J.W., 2023. A temperature-responsive intravenous needle that irreversibly softens on insertion. Nat. Biomed. Eng. https://doi.org/10.1038/s41551-023-01116-z.

Azizi, A., Tremblay, C.C., Gagné, K., Martel, S., 2019. Using the fringe field of a clinical MRI scanner enables robotic navigation of tethered instruments in deeper vascular regions. Sci. Robot. 4 (36). https://doi.org/10.1126/scirobotics.aax7342.

Hong, A., Petruska, A.J., Zemmar, A., Nelson, B.J., 2021. Magnetic control of a flexible needle in neurosurgery. IEEE Trans. Biomed. Eng. 68 (2). https://doi.org/10.1109/TBME.2020.3009693.

Hu, X., Hu, Q., He, Y., Yi, X., Wu, Z., Hu, H., Ouyang, Y., Yu, F., Peng, M., 2024. Efficacy and safety of microwave ablation and its synergistic potential in the treatment of early-stage non-small cell lung cancer. Clin. Imag. https://doi.org/10.1016/j.clinimag.2023.110070.

Kim, Y., Parada, G.A., Liu, S., Zhao, X., 2019. Ferromagnetic soft continuum robots. Sci. Robot. 4 (33), 1–16. https://doi.org/10.1126/SCIROBOTICS.AAX7329.

Kim, Y., Genevriere, E., Harker, P., Choe, J., Balicki, M., Regenhardt, R.W., Vranic, J.E., Dmytriw, A.A., Patel, A.B., Zhao, X., 2022. Telerobotic neurovascular interventions with magnetic manipulation. Sci. Robot. 7 (65), eabg9907. https://doi.org/10.1126/scirobotics.abg9907.

Kuntz, A., Emerson, M., Ertop, T.E., Fried, I., Fu, M., Hoelscher, J., Rox, M., Akulian, J., Gillaspie, E.A., Lee, Y.Z., Maldonado, F., Webster, R.J., Alterovitz, R., 2022. Autonomous medical needle steering. In Vivo 7614, 1–14. https://doi.org/10.1126/scirobotics.adf7614.

Lee, W., Nam, J., Kim, J., Jung, E., Kim, N., Jang, G., 2021. Steering, tunneling, and stent delivery of a multifunctional magnetic catheter robot to treat occlusive vascular disease. IEEE Trans. Ind. Electron. 68 (1). https://doi.org/10.1109/TIE.2020.2965480.

Li, P., Wang, Z., Ye, C., Fang, D., Zhang, J., Liang, C., 2024. Development and verification of a micro magnetically guided helical robot with active locomotion and steering capabilities for guidewires. Sensors Actuators A Phys 369. https://doi.org/10.1016/j.sna.2024.115123.

Lou, L., Ramakrishna, K., Shao, L., Park, W.T., Yu, D., Lim, L., Wee, Y., Kripesh, V., Feng, H., Chua, B.S.Y., Lee, C., Kwong, D.L., 2010. Sensorized guidewires with MEMS tri-axial force sensor for minimally invasive surgical applications. In: 2010 Annual International Conference of the IEEE Engineering in Medicine and Biology Society. EMBC'10, pp. 6461–6464. https://doi.org/10.1109/IEMBS.2010.5627345.

Makevnina, V.V., 2018. Solid-state modeling of human tracheobronchial tree for 23 generations of airways. J. Phys. Conf. 1124. https://doi.org/10.1088/1742-6596/1124/3/031002.

Natale, A., Reddy, V.Y., Monir, G., Wilber, D.J., Lindsay, B.D., McElderry, H.T., Kantipudi, C., Mansour, M.C., Melby, D.P., Packer, D.L., Nakagawa, H., Zhang, B., Stagg, R.B., Boo, L.M., Marchlinski, F.E., 2014. Paroxysmal AF catheter ablation with a contact force sensing catheter: results of the prospective, multicenter SMART-AF trial. J. Am. Coll. Cardiol. 64 (7). https://doi.org/10.1016/j.jacc.2014.04.072.

Piskarev, Y., Sun, Y., Righi, M., Boehler, Q., Chautems, C., Fischer, C., Nelson, B.J., Shintake, J., Floreano, D., 2024. Fast-response variable-stiffness magnetic catheters for minimally invasive surgery. Adv. Sci. 11 (12). https://doi.org/10.1002/advs.202305537.

Rose, S.C., Thistlethwaite, P.A., Sewell, P.E., Vance, R.B., 2006. Lung cancer and radiofrequency ablation. J. Vasc. Intervent. Radiol. https://doi.org/10.1097/01.RVI.0000222707.44902.66.

Tiryaki, M.E., Elmacioğilu, Y.G., Sitti, M., 2023. Magnetic guidewire steering at ultrahigh magnetic fields. Sci. Adv. 9 (17). https://doi.org/10.1126/sciadv.adg6438.

Wang, L., Guo, C.F., Zhao, X., 2022. Magnetic soft continuum robots with contact forces. Extrem. Mech. Lett. 51, 101604. https://doi.org/10.1016/j.eml.2022.101604.

Yang, X., Shang, W., Lu, H., Liu, Y., Yang, L., Tan, R., Wu, X., Shen, Y., 2020. An agglutinate magnetic spray transforms inanimate objects into millirobots for biomedical applications. Sci. Robot. 5 (48), 1–13. https://doi.org/10.1126/scirobotics.abc8191.

Yang, Q., Enríquez, Á., Devathasan, D., Thompson, C.A., Nayee, D., Harris, R., Satoski, D., Obeng-Gyasi, B., Lee, A., Bentley, R.T., Lee, H., 2022. Application of magnetically actuated self-clearing catheter for rapid in situ blood clot clearance in hemorrhagic stroke treatment. Nat. Commun. 13 (1). https://doi.org/10.1038/s41467-022-28101-5.

Yang, Z., Yang, H., Cao, Y., Cui, Y., Zhang, L., 2023. Magnetically actuated continuum medical robots: a review. Advanced Intelligent Systems. https://doi.org/10.1002/aisy.202200416.

Zhang, T., Yang, L., Yang, X., Tan, R., Lu, H., Shen, Y., 2021. Millimeter-scale soft continuum robots for large-angle and high-precision manipulation by hybrid actuation. Adv. Intell. Syst. 3 (2), 2000189. https://doi.org/10.1002/aisy.202000189.

Zhou, C., Yang, Y., Wang, J., Wu, Q., Gu, Z., Zhou, Y., Liu, X., Yang, Y., Tang, H., Ling, Q., Wang, L., Zang, J., 2021. Ferromagnetic soft catheter robots for minimally invasive bioprinting. Nat. Commun. 12 (1), 1–12. https://doi.org/10.1038/s41467-021-25386-w.